Sensors & Actuators: B. Chemical 379 (2023) 133261

Contents lists available at ScienceDirect

Sensors and Actuators: B. Chemical

journal homepage: www.elsevier.com/locate/snb

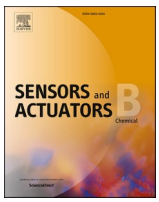

High-performance fluorescent and colorimetric dual-mode nitrite sensor boosted by a versatile coumarin probe equipped with diazotization-coupling reaction-sites

Tianshi Zhang [a,b], Yuan Liu [a,*], Jiguang Li [a,b], Wenfei Ren [a,b], Xincun Dou [a,b,**]

[a] Xinjiang Key Laboratory of Explosives Safety Science, Xinjiang Technical Institute of Physics and Chemistry, Chinese Academy of Sciences, Urumqi 830011, China
[b] Center of Materials Science and Optoelectronics Engineering, University of Chinese Academy of Sciences, Beijing 100049, China

ARTICLE INFO

Keywords:
Nitrite
Colorimetric
Fluorescent
Diazotization
Coupling reaction

ABSTRACT

Nitrite has posed ubiquitous threats to the environment, human health, and public security because of its crucial role in food processing, construction, farming, and explosive manufacturing industries. To achieve accurate, sensitive, and on-site detection of trace nitrite, a colorimetric-fluorescent dual-mode sensing probe with unique photophysical process was designed for ultrasensitive determination of nitrite by precisely adjusting the amino site and significantly influencing the coupling reaction activity. This modulating strategy breaks through the dilemma of azo-product with only colorimetric phenomenon, facilitating the probe, 7-amino-4-methylcoumarin, to maintain a desirable sensitivity with detection limits of 98 nM and 629 nM in fluorescent and colorimetric modes, respectively, as well as an outstanding specificity even in the presence of 15 common anions and interfering substances. The probe was further integrated into a portable sensor by applying a polyvinyl alcohol hydrogel as a loading substrate, which showed superior sensing performances in analyzing nitrite in various real samples with visualized, anti-interferent, and dual-mode responses. Consequently, the present reaction-site modulation strategy would provide a general reference for ultrasensitive, on-site, and visual detection of nitrite, and it can be broadly applied in environmental monitoring and food safety assessment.

1. Introduction

Nitrite, a pivotal component of the natural environment, plays an important role in food additives, concrete admixtures, and soil-nitrogen cycling [1–3]. However, its long-term accumulation could endanger human health (e.g., carcinogenesis) and induce water/soil pollution; therefore, nitrite has been stipulated as a highly toxic substance by the World Health Organization (WHO) [4]. Furthermore, nitrite is a strong oxidant component in improvised explosives and is one of the main degradation components of common high-energy explosives (nitro-aromatic hydrocarbons, nitramines, and nitrates) [5–7]. Hence, there is a pressing demand for on-site detection of trace nitrite to maintain sustainable environmental development as well as safeguard public health and security [8–11]. To date, intensive efforts have been devoted to quantifying nitrite at sub-micromolar levels, such as capillary electrophoresis, spectrophotometry, electrochemical detection, and ion chromatography [12–15]; although most of these methods work well in laboratory settings, they are not easily translocated for on-site, real-time measurements. Additionally, some commercially available dipstick strips rely on the inexpensive and user-friendly Griess method, including two indicators, sulfanilamide and N-(1-naphthyl)-ethylenediamine, with colorimetric quantitation through a comparison of the color scale by naked-eye observation on the formation of a highly colored azo-dye in the presence of nitrite [16–20]. However, several issues cannot be avoided when considering the stability and repeatability of nitrite detection: (i) the para- unsubstituted aromatic amine as a diazotization reagent is easily oxidized to quinone imine structure in air, making it difficult to maintain long-term stability owing to the denaturation; (ii) Upon the acidic environment of the diazotization reaction, the nitrite with strong oxidation present a higher requirement in structural stability for reacting with the diazotization reagent; (iii) The influence of ambient light interferes with the quantitation accuracy of nitrite based on

* Corresponding author.
** Corresponding author at: Xinjiang Key Laboratory of Explosives Safety Science, Xinjiang Technical Institute of Physics and Chemistry, Chinese Academy of Sciences, Urumqi 830011, China.
E-mail addresses: liuyuan@ms.xjb.ac.cn (Y. Liu), xcdou@ms.xjb.ac.cn (X. Dou).

https://doi.org/10.1016/j.snb.2022.133261
Received 3 November 2022; Received in revised form 27 December 2022; Accepted 27 December 2022
Available online 28 December 2022

chromogenic reaction. Thus, these issues significantly limit the wide application of the Griess method involving a technique/device and further raise an urgent demand for a highly sensitive, stable, and easy-to-use analytical strategy to meet the practical needs for efficient and visual detection of nitrite.

With this aim, specifically to meet the requirement of highly sensitive on-site detection toward nitrite, an effective strategy is to construct a sensing platform equipped with a dual-mode response, such as colorimetry and fluorescence, to provide a more intuitive visualization effect and higher sensitivity. Generally, the fluorescence technique is superior, with a more sensitive response for quantifying trace substances, and colorimetry possesses better operability without extra laser excitation and a dark environment, as well as a more straightforward coloring result [21]. In most cases, azo-dyes exhibit only chromogenic phenomena and the photophysical processes of the azo-dyes are not well clarified [22,23]. Several mechanisms are responsible for the fluorescence generation and its optical property variations (e.g., fluorescence turn-on, turn-off and ratiometric change), which include photoinduced electron transfer, excited state intramolecular proton transfer, twisted intramolecular charge transfer, fluorescence resonance energy transfer, and aggregation-caused quenching or aggregation-induced enhancement [24–30]. To date, many studies claim that the chromogenic phenomenon of the azo-dye comes from the charge transfer between n and π* [31], whereas some cases infer that it is relevant to the alteration of the molecular conformation [32]; however, how the latter acts on the photophysical process remains unexplored. Therefore, an investigation of the molecular conformation change is beneficial and promising to reveal its influence on the mechanism of the photophysical change and further guide the regulation of the molecular structure, consequently realizing fluorescence generation and colorimetric-fluorescent dual-mode detection.

Herein, to solve the bottleneck issue of nitrite on-site detection, we designed a coumarin probe equipped with both diazotization and coupling reaction sites, finally achieving colorimetric-fluorescent dual-mode detection toward nitrite with desirable performance. Starting with modulation of the amine site to affect the diazotization reaction activity, the subsequent coupling reaction sites were altered accordingly. Diazotization and coupling reactions occur simultaneously in one system with blue fluorescence turn-off and yellow colorimetry. The photophysical characteristics of the dual-mode response were verified by analyzing the dihedral angle, energy distribution, transition charge density and dipole density of the product. Furthermore, the probe was anchored within a polyvinyl alcohol (PVA) hydrogel substrate to construct a portable sensor that could be applied for nitrite detection in real samples with excellent outcomes, demonstrating the applicability and reliability of the strategy in practical scenarios.

2. Experimental section

2.1. Materials and chemicals

Polyvinyl alcohol (PVA), sodium thiosulfate ($Na_2S_2O_3$), sodium hydroxide (NaOH), acetonitrile (MeCN), dimethyl sulfoxide (DMSO) and acetic acid were bought from Shanghai Aladdin Biochemical Technology Co. Ltd. Potassium persulfate (KPS) was purchased from Tianjin Zhiyuan Chemical Reagent Co. Ltd. Lithium chloride (LiCl), sodium bromide (NaBr), sodium chloride (NaCl), potassium sulfate (K_2SO_4), methanol (MeOH), ethanol (EtOH) and tetrahydrofuran (THF) were purchased from Sinopharm Chemical Reagent Co. Ltd., and all chemical compounds were used as received without further purification.

2.2. Computation method

All ground state geometric structures (S_0) of the probe and the reaction product were fully optimized using the PBE0 [33] exchange correlation functional with Grimme's DFT-28D3(BJ) empirical dispersion correction [34]. The 6–31G(d) basis set [35] was adapted for all atoms. The structures of the lowest singlet excited state (S_1) of the probe and the reaction product were optimized based on the time-dependent density functional theory (TD-DFT) at PBE0-D3 (BJ)/6–31G(d) level approach to evaluate the vertical emission energies since PBE0 functional is found to provide a good balance between the local excited and the intramolecular charge transfer (ICT) states, with average absolute errors of ca 0.14 eV for the low-lying excited states of the conjugated organic compounds. The linear response polarizable continuum model (PCM) [36] was used to optimize the geometry of the singlet ground state and excited state of the probe and the reaction product considering the solvent environment. All the computation were calculated using Gaussian 09 [37] program package. The wave function analysis including the optimal geometric configuration, the highest occupied/lowest unoccupied molecular orbital (HOMO/LUMO) energy, electron hole analysis, transition dipole moment, transition density, electrostatic potential and average local ionization energy [38–40] of the probe were produced by the Multiwfn program [41], while the iso-surfaces mapping were rendered by VMD software [42].

3. Results and discussion

3.1. Detection mechanism of the colorimetric-fluorescent coumarin probe

Coumarin is a fluorophore of lactone bound to the benzene ring with a large π-conjugated structure, which can diazotize with nitrite and activate a coupling reaction by modifying the amino group on the benzene ring (Fig. 1a). The diazotization reactivity between nitrite and the amino group at different sites could be investigated using the natural bond orbital method to evaluate the electrostatic potential surface (EPS) of the coumarin molecule (Fig. S1). When the amino group is at position 7, its EPS is relatively high, indicating that the amino group at this site is less negatively charged and is more susceptible to nucleophilic attack by nitrite. From the average local ionization energy analysis, it can be observed that the ortho-amino position at the benzene is more likely to take place the coupling reaction. Based on the computation results of the oscillator strengths (f) of these coumarin molecules, it was established that the amino group substituted at site 7 ranked as the largest with an f value of 0.6429, implying that the coumarin molecule with an amino group at site 7 had the highest fluorescence intensity (Table S1). The electron-hole analysis of the coumarin molecules shows that both of the electron-hole overlap (Sr) and distance parameter of electron-hole center (D) for the 7-amino coumarin molecule are relatively larger, indicating that both the electron-hole overlap and the electron hole distribution range are large (Table S2, Fig. S2). For the reaction between the coumarin probe and nitrite, the product could undergo different coupling reactions at different sites. As calculated, the binding energy of site 6 (120.38 kJ/mol) is significantly higher compared to those of sites 5 (90.93 kJ/mol) and 8 (111.47 kJ/mol), which means that the more advantageous coupling reaction occurred at the ortho-carbon of the amino group (Fig. 1b) [43]. From the contribution of the molecular orbital to the molecular absorption spectrum, it can be observed that the main transition is from the charge transfer of the amino group (Fig. S3).

From the contribution of the molecular orbitals to the emission spectrum, it can be observed that the main contribution of the $S_1 \rightarrow S_0$ electronic transition is controlled by the HOMO and LUMO orbitals. The electrons are mainly distributed on coumarins, resulting in local excitation and fluorescence emission (Fig. 1c). After the diazotization-coupling reaction between coumarin and nitrite, the two coumarin probe molecules were bonded through the azo-bond. From the contribution of the molecular orbital to the molecular absorption spectrum, it can be observed that the main transition originates from the local excitation of π-π* on the benzene ring, which is mainly controlled by the HOMO-1 and LUMO orbitals. The emission oscillator intensity in the orbital contribution analysis of the emission spectra is 0.0006, which means that the products have no fluorescence, proving that detection

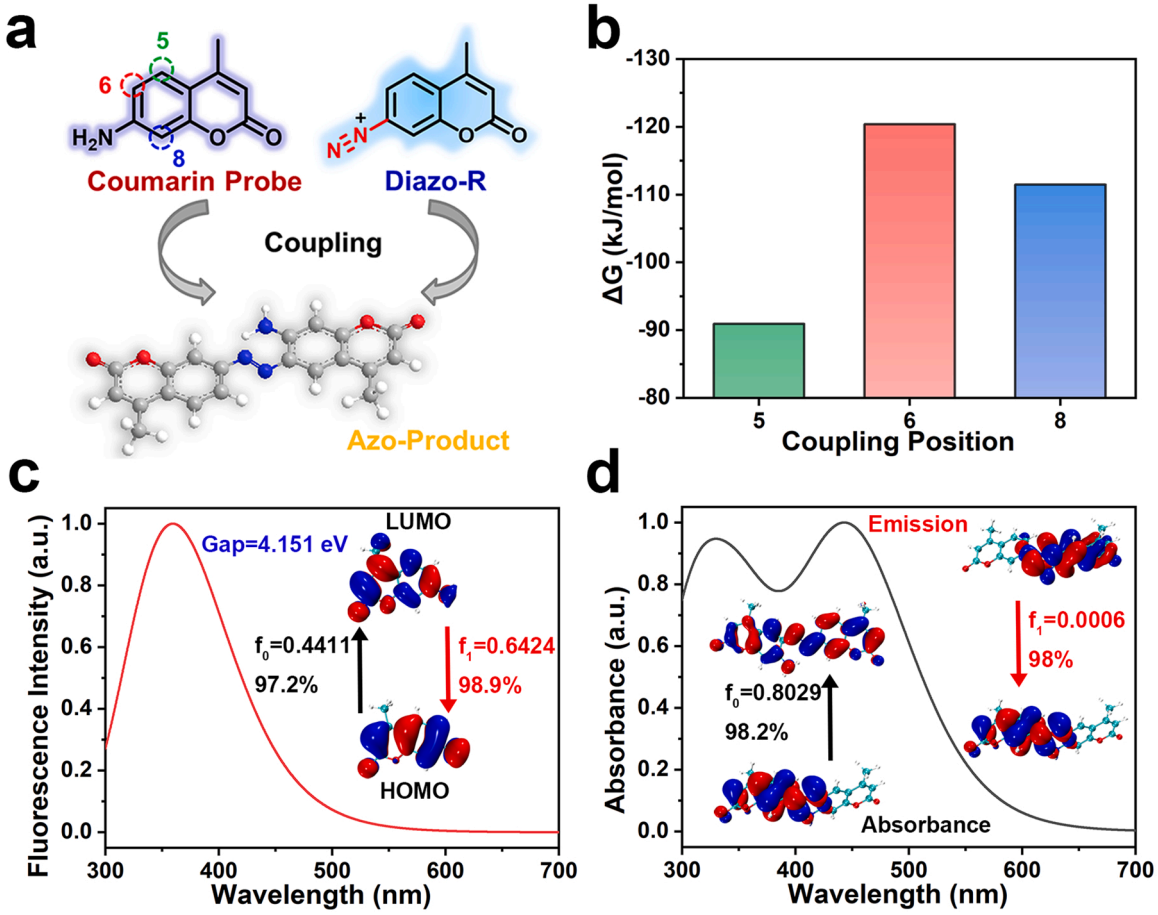

Fig. 1. (a) Schematic illustration of the probe modulation strategy for detecting nitrite upon the diazotization and coupling interaction. (b) Histogram of the free energy of coupling reaction sites at 5, 6, and 8 of the coumarin probe. (c) The contribution of the molecular orbital of the coumarin probe to the fluorescent emission. (d) The contribution of the molecular orbital of the reaction product to the absorption spectra.

reaction induces fluorescence quenching (Fig. 1d). Hence, the fluorescent 7-amino-4-methylcoumarin probe can be quenched when it reacts with nitrite, and a colorimetric phenomenon is generated when the azo-bond is formed between the intermediate product and another probe molecule. This reaction mechanism can be applied to specifically recognize nitrite in a colorimetric-fluorescent dual-mode response.

3.2. Detection properties of the coumarin probes toward nitrite

To design a reasonable reaction environment, the emission spectra of the fluorescent coumarin probe molecule in solvents with different polarities (water mixed with DMSO, methanol, ethanol, acetonitrile, and THF at a ratio of 1:1) were studied. The coumarin probe exhibited fluorescence quenching and color change within 10 s, except in the acetonitrile system (Fig. S4 and S5). It can be observed that the ethanol system changes significantly after reacting with nitrite with a high quenching efficiency of 99.5 % (Fig. 2a). This is because the proton-type solvent is conducive to the diazotization reaction, and the polarity of ethanol can prevent excessive solvation of electrophilic reagents and affect the coupling reaction. Therefore, a combination of water and ethanol (v:v = 1:1) with the most evident quenching efficiency and color change was selected as the optimal solvent system for subsequent studies. Under this condition, the fluorescence lifetime of the coumarin probe is 4.89 ns, verifying that the fluorescence of the coumarin probe belongs to radiation recombination (Fig. S6), and the fluorescence lifetime did not change significantly after the reaction (4.24 ns), indicating that the fluorescence quenching process belongs to the intramolecular charge transfer mechanism.

To investigate how the coumarin probe reacts with nitrite over time, the changes in the quenching efficiency and absorbance of the reaction were recorded for 10 min (Fig. 2b). With 4 mM nitrite, the absorbance at 450 nm and quenching efficiency at 446 nm of the probe solution changed rapidly, increased linearly within 4 min, and finally reached a peak within 10 min. This illustrates that the response time is 60 s (Supplementary Movie S1), and the visualized phenomenon stabilized after 10 min. Subsequently, the concentration-dependent fluorescence of the coumarin probe was studied in the presence of nitrite at concentrations ranging from 0 to 100 μM (Fig. S7a). The fluorescence spectra versus increased nitrite concentration displayed various lowered fluorescence peaks at 446 nm (Fig. 2c). The linear fitting of the quenching efficiency at 446 nm ($1-I/I_0$) versus the nitrite concentration showed a good linear relationship with a coefficient value $R^2 = 0.9867$, where I_0 and I represented the fluorescence intensity before and after nitrite addition, respectively. The limit of detection (LOD) was calculated as 98 nM with a linear range of 8–80 μM ($3\sigma/k$, normalized $\sigma = 0.00022$). In addition, in colorimetric mode, a color change trend of the probe solution from colorless to bright orange was observed (Fig. S7b), and the absorption spectra exhibited a strong peak at 450 nm. The absorbance linearly correlated with the nitrite concentration in 8–100 μM with a coefficient value of $R^2 = 0.9928$ and a calculated LOD of 629 nM ($3\sigma/k$, normalized $\sigma = 0.001$, Fig. 2d). Compared with previous reports, the present coumarin probe possesses good sensitivity and detection range in both fluorescent and colorimetric modes (Table S3), and the sensitivities in both modes are adequate to meet the safety threshold (65 μM) stipulated by WHO [44].

Supplementary material related to this article can be found online at

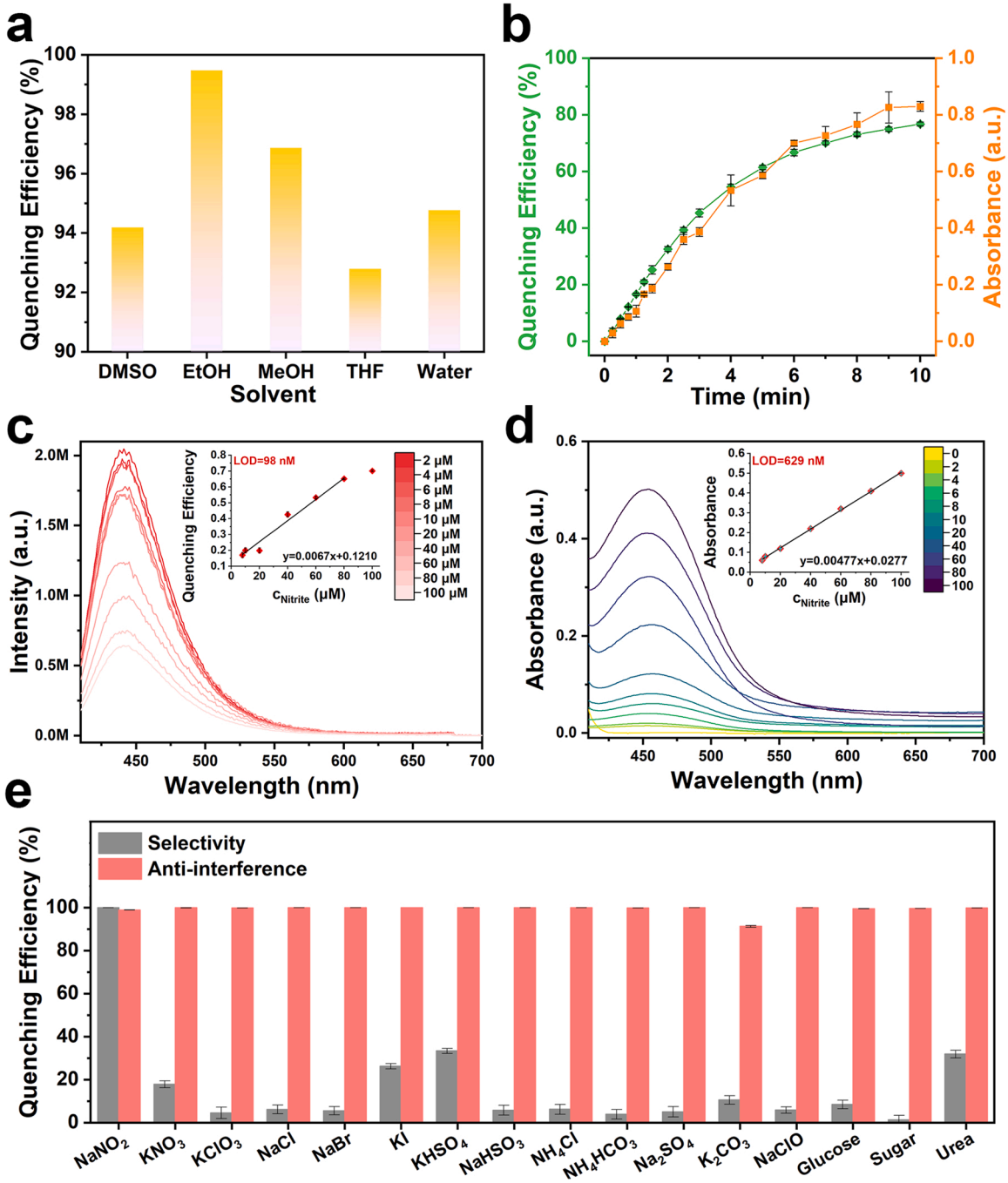

Fig. 2. (a) Fluorescence quenching efficiency of the coumarin probe in different solvents. (b) The trends of the quenching efficiency and absorbance of the coumarin probe over time in the presence of 1 mM nitrite. (c) The corresponding relationship between the nitrite concentration and fluorescence intensity (λ_{Ex} = 395 nm, λ_{Em} = 446 nm). (d) The corresponding relationship between the increasing nitrite concentration and the absorbance. (e) The specificity and the anti-interference properties of the coumarin probe toward nitrite upon the evaluation of the quenching efficiency.

doi:10.1016/j.snb.2022.133261.

Furthermore, to explore the specificity and anti-interference capability of the coumarin probe in detecting nitrite, 15 oxidants, reductants and other anionic substances (0.1 M) were selected as the interfering substances. For the specificity study, it can be observed that the probe does not exhibit coloring change and fluorescence quenching as shown in both colorimetric and fluorescent images when the above interfering substances were added, except for nitrite (Fig. S8a,b). When the probe solution contained a mixed solution containing nitrite and these interfering substances at a concentration ratio of 1:10 (0.01 M:0.1 M), all probe solutions turned into orange and showed a fluorescence quenching phenomenon, suggesting that both the colorimetric and fluorescent responses of the probe toward nitrite were not significantly disturbed (Fig. S8 c,d). Upon statistical analysis of the quenching efficiency, except that the fluorescence of the probe solution containing nitrite completely disappeared with a quenching efficiency of 99.97 %, all the quenching efficiencies of the probe solutions involving interfering substances remained at a low level in the specificity test (Fig. 2e). These results confirm that the probe possesses excellent specific recognition of nitrite and holds great anti-interference capability for detecting nitrite in the presence of other interfering substances. In addition, to verify the long-term stability of the coumarin probe, its effect toward nitrite was

evaluated during a storage period of 0–6 months. It is clear from the optical images in both colorimetric and fluorescent modes that the phenomena of the same probe solution toward 1 mM nitrite are almost identical (Fig. S9a), and the quenching efficiency of all samples with different storage times varied in a narrow range from 99.03 to 99.71 with a relative standard deviation (RSD) of 0.26 % (Fig. S9b). Furthermore, it was found that stable colorimetric and fluorescent detection phenomena can be maintained within the range of pH 1–13 (Fig. S10a, b), and the reagent still maintained the same colorimetric and fluorescent properties at 50 °C (Fig. S10c,d). These results prove that the coumarin probe has good stability in the combined water/ethanol solvent system for more than 6 months, suggesting detection reliability in long-term applications.

3.3. Structural analysis of the diazotization-coupling reaction products

To determine the reason for the fluorescence quenching process, the C-N = N-C dihedral angle of the azo-bond in the product was scanned. With an increasing dihedral angle, the energy of S_0 decreased until the dihedral angle reached 180°. Thus, the most stable configuration of the reaction product occurred when the two coumarin molecules were nearly parallel, leading to charge transfer (Fig. 3a). The energy of the S_1 system fluctuates slightly with the dihedral angle and relaxed to 95°, indicating that the system is affected vertically by the rotation of the N-N bond in the excited state. The fragment transition density matrix heat map could be obtained by dividing the azo-product into three pieces (Fig. 3b), from which it can be observed that the hole distribution in the x-axis is predominantly located in fragments 1 and 2 with a clear red color. Conversely, the electron distribution in the y-axis is located mainly in fragments 2 and 3, revealing that electrons transfer from fragments 1and 2 to fragments 2 and 3 (from one coumarin molecule to the other through the azo-bond). From the transition charge density distribution diagram (Fig. S11), it can be observed that both the positive (green region) and negative (pink region) positions are locally distributed around the azo-bond, which indicates that the azo-bond acts as a bridge to connect the charge transfer process between the two coumarin molecules (from fragment 1 to fragment 3). This local transition feature originates from the ordered distribution of electrons (blue region) and holes (green region in Fig. 3c), where the electrons are preferentially distributed on the side of fragment 3 and the azo-bond, whereas the holes are predominantly distributed on the side of fragment 1 and the azo-bond. It is further verified that there is an intramolecular charge transfer from the separation degree of electrons and holes because the distance parameter of the electron-hole center D is 3.341 Å (Fig. 3d), indicating that electron transfer is favored in the structure. Therefore, it was confirmed that the 7-amino group-substituted coumarin probe reacted with nitrite and generated fluorescence quenching and color. This is because the twisted molecule caused by the C=N bond conformation has an intermolecular charge transfer owing to the large electron-hole separation.

3.4. Construction of the hydrogel sensor for nitrite detection in real samples

To realize the on-site nitrite detection in practical scenarios, a hydrogel sensor was designed by anchoring the coumarin probe into white PVA hydrogels, which were further assembled on a flexible thermoplastic polyurethane (TPU) substrate (Fig. 4a-i); one PVA hydrogel served as the module for direct sensing and the other served as the reference. The white PVA hydrogel provided a good non-interference background, and its micro-level pore size ensured adequate adsorption toward the probe molecules and prevented them from diffusing into the sample solution during detection (Fig. 4a-ii). A color change from white to yellow and quenched blue fluorescence were observed owing to the specific identification of the probe-loaded hydrogel to nitrite (Fig. 4a-iii). To evaluate the reaction time of the hydrogel sensor, it was half-inserted into a 1 mM nitrite solution, and fluorescence images were recorded at an interval of 20 s (Fig. S12a). The difference image (D-image) and the histogram equalized image (Histeq image) were obtained by the difference processing of the images from the sensing module and the reference module to reflect the difference before and after detection. Through gray scale analysis, it was established that the fluorescent signal is stable after 1 min, and its color value obeys the negative exponential law (similar to the first-order reaction) with

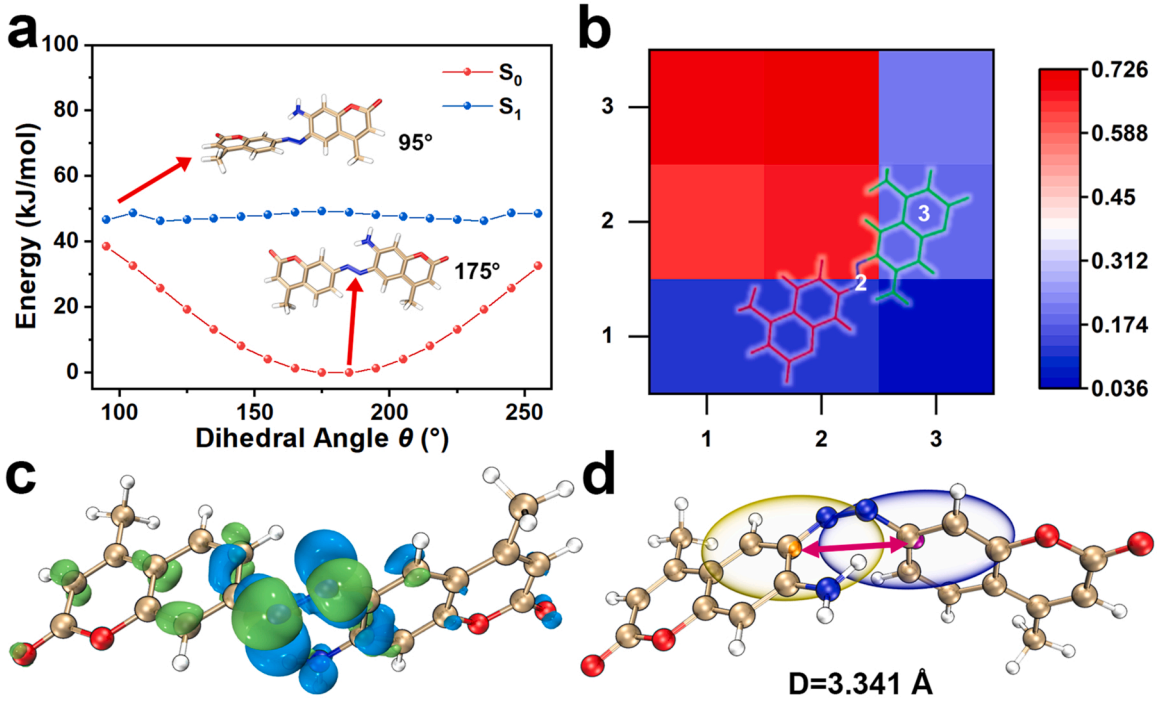

Fig. 3. (a) Curve of the product energy with C-N = N-C dihedral angle θ. (b) Heat map of the energy distribution in different parts of the reaction product. (c) The transition charge density and (d) the transition dipole density of the reaction product.

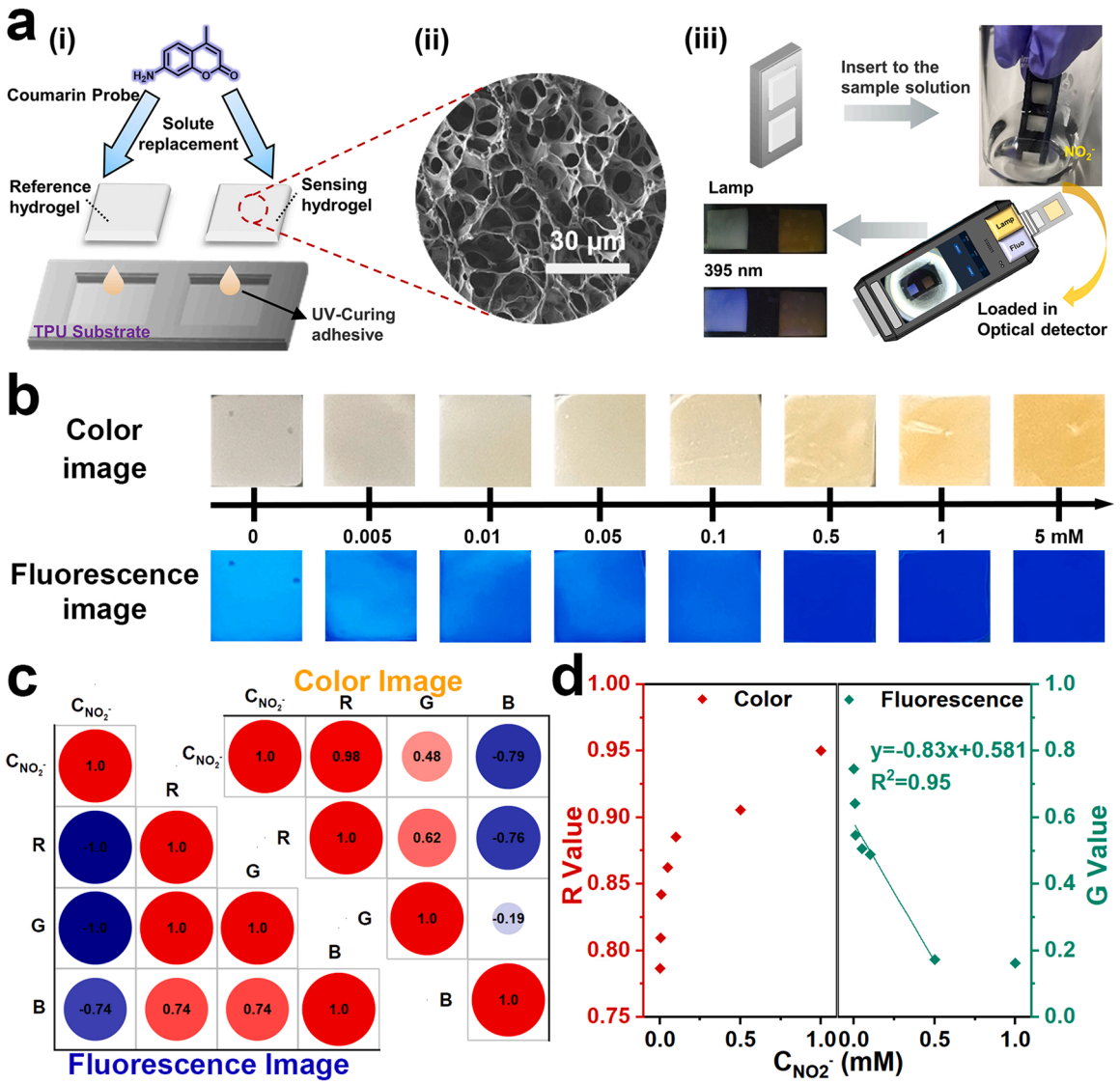

Fig. 4. (a) i) Construction of the coumarin probe loaded PVA hydrogel sensor for nitrite detection. ii) SEM image of the PVA hydrogel. iii) Scheme of the hydrogel sensor applied for detecting liquid sample. (b) The images of the hydrogel sensor used to detect nitrite solutions with different concentrations under natural light and an excitation of 395 nm. (c) Correlation analysis of the concentration of nitrite and the value of R, G, and B in color and fluorescence images. (d) The relationship between the extracted RGB values of images for the hydrogel sensor after detecting different concentrations of nitrite solutions.

respect to time, which is more suitable for the quantitative analysis (Fig. S12b) [45]. To explore the quantitative capability of the hydrogel sensor by numerically analyzing the visual signal, the sensor was placed in 0, 0.005, 0.01, 0.05, 0.1, 0.5, 1, and 5 mM nitrite solutions, and the corresponding optical images were recorded. With an exposure time of 90 s, the colorimetric and fluorescent modes showd significant changes (Fig. 4b). Through the correlation analysis of the nitrite concentration and the corresponding RGB values of the images, it can be seen that R value is more suitable for analyzing the colorimetric image as the correlation coefficient of R is equal to 0.98 (closer to ± 1). For the fluorescent image analysis, although the G and R values are equal to − 1, the G value changes significantly and has a smaller relative deviation than the R value, indicating a higher reliability. Thus, the G value is more suitable for the fluorescent image analysis (Fig. 4c). After extracting and analyzing the RGB values of the images, it was found that although the R value of the colorimetric image was related to the concentration, it did not have a good linear feature to support a quantitative analysis (Fig. 4d). The G value of the fluorescent image is linear within the nitrite concentration range from 0.05 mM to 5 mM, and the detection limit is 1.42 μM, which is lower than the safety threshold of 65 μM (WHO), suggesting that this method possesses good quantitative capability for on-site nitrite analysis.

To investigate the specificity of the hydrogel sensor to differentiate nitrite and the potential co-existing interferents, images under both natural light and 395 nm excitation were taken after the hydrogel sensing module was applied to detect nitrite and other interferents (Fig. 5a, b). All images of the interferents showed negligible effects on the hydrogel sensing module, whereas apparent yellow coloring and fluorescence quenching were observed after the sensor was used for detecting the nitrite solution, which could also be verified from the RGB value extraction analysis for the above images (Fig. 5c). For colorimetric analysis, the B value is more appropriate for differentiating yellow (after reaction) from white (before reaction or non-reaction). In terms of fluorescence, the quenching is mainly reflected as brightness reduction in images, which can be calculated as:

$$V_B = 0.547 \times \sqrt[2.2]{R^{2.2} + (1.5G)^{2.2} + (0.6B)^{2.2}}$$

where V_B is brightness value; R, G, and B correspond to the normalized color values of the image [46]. The change in G had the largest impact

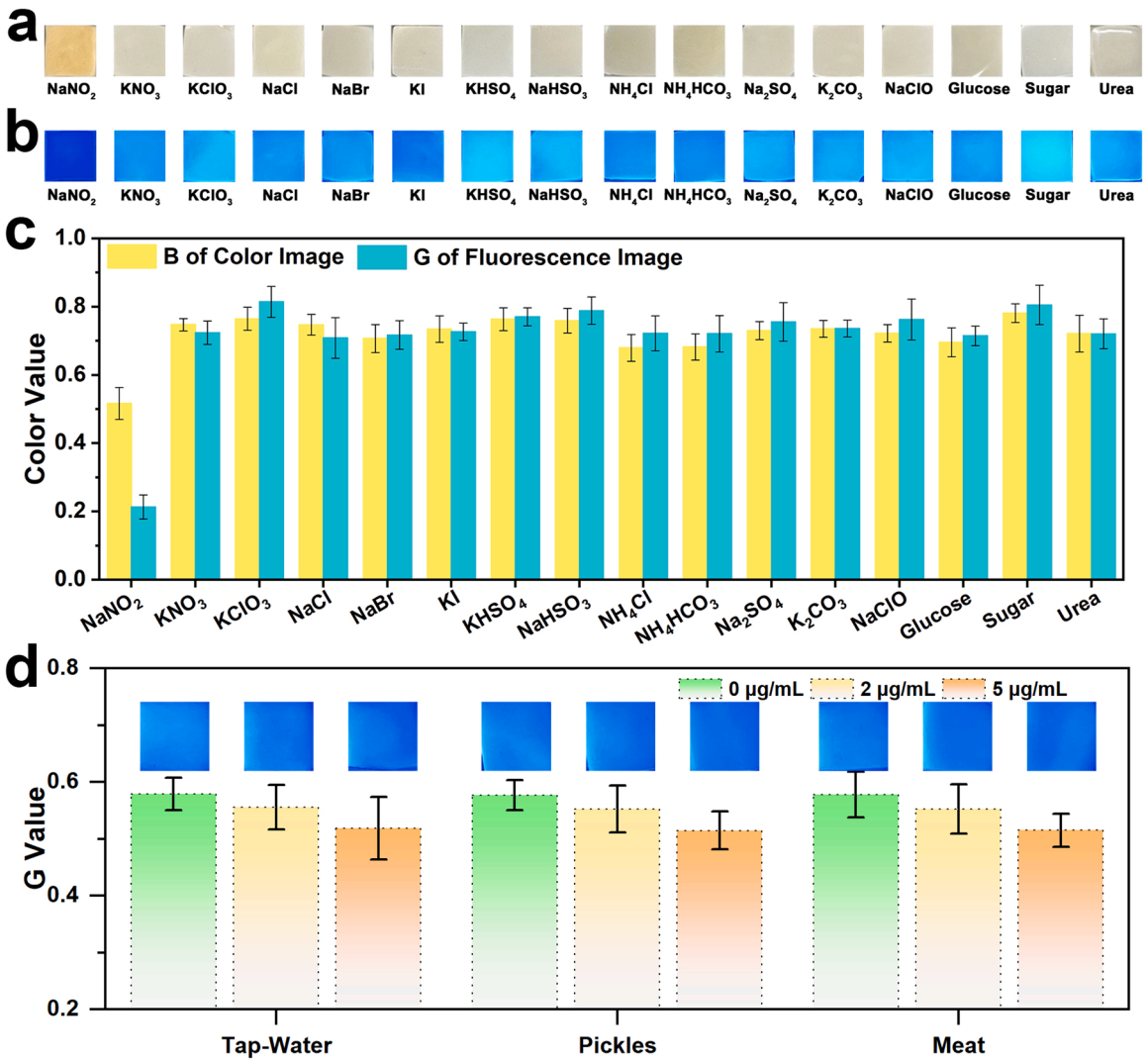

Fig. 5. Images for specificity study of the hydrogel sensor towards nitrite and other 15 interferents under (a) natural light and (b) an excitation of 395 nm. (c) The extracted RGB values of the colorimetric and fluorescent images in the specificity study. (d) The evaluation of the hydrogel sensor for the nitrite spiked in real samples upon the G value analysis of the fluorescence images.

on brightness, verifying that the G value from the correlation analysis shown in Fig. 4c had the highest relevance with the concentration-dependent fluorescence images. To explore the practicability of the hydrogel sensor, it was applied to detect nitrite spiked in tap-water, pickles, and sausages. Nitrite at different concentrations (0, 2 and 5 μg/mL) was spiked into standardized samples and tested by the hydrogel sensor and spectrophotometry method specified in the China National Standard (GB5099.33–2016). With duration of 5 min, it can be clearly observed by the naked eye that the hydrogel sensors in samples with 2 and 5 μg/mL nitrite displayed clear yellow coloring (Fig. S13). Furthermore, by comparing the G values of the fluorescence images of the sensing module, it was established that the images for the same concentration of nitrite spiked in different samples showed a similar fluorescence quenching and G value reduction (Fig. 5d).

Thus, to demonstrate the reliability of the sensing method, the nitrite content based on the G value extracted from the fluorescent image was compared with that measured through spectrophotometry. It can be observed that the measured values of this sensing method are close to those from the standard spectrophotometry method (Table S4), showing the recovery varying from 103.6% to 120% and the RSD basically less than 10%. These results indicate that the proposed sensing method is highly accurate and reliable for analyzing real samples, and that the hydrogel sensor is promising for on-site nitrite analysis.

3.5. *Qualitative analysis for trace nitrite particulates*

In addition, because of the liquid micro-environment of the hydrogel substrate, the sensor can adsorb and dissolve airborne trace nitrite solid particles in gaseous test, and then accomplish the reaction and produce optical signal changes (Fig. 6a). With the exposure of the hydrogel sensor to vapor with nitrite solid particles, the image could be captured using a video camera under specific optical conditions. As the background of fluorescence quenching detection is not a complete dark-field, the simulated dark field image was obtained by differential processing of the sensing module image and the reference module image (Fig. 6b). Furthermore, through correlation analysis of the image and R, G, and B values, it was established that G value could dominantly represent the information of the fluorescent image. By adjusting the input color scale of G, the corresponding D-image can be output and the reaction area and color map can be analyzed through further pixel sampling and scanning. It has been verified that if the G value is larger than 0.04, the reaction with nitrite occurs in the corresponding area. To test the responsiveness of the hydrogel sensor to solid samples, a time-dependent recognition test on solid nitrite particles was conducted. Significant quenching

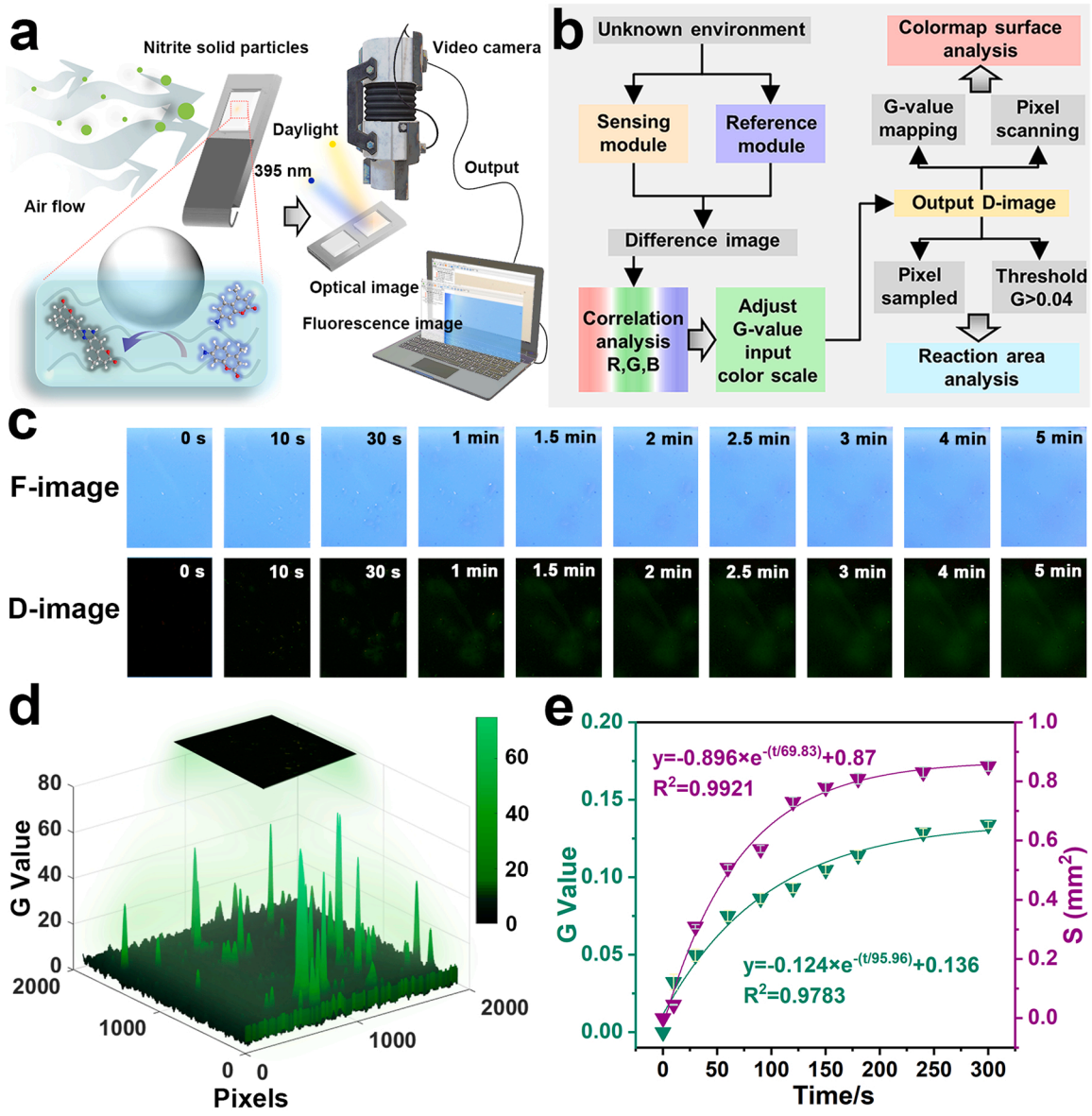

Fig. 6. (a) Schematic illustration of the analysis of nitrite solid particles via the hydrogel sensor. (b) Flow chart of the fluorescence image analysis from hydrogel sensor after detecting nitrite solid particles. (c) Time-dependent fluorescence images (F-image) and difference images (D-image) of the hydrogel sensor for analyzing trace nitrite solids. (d) 3D colormap surface analysis of the output D-image. (e) G value and fluorescence area in the difference image as a function of the reaction time.

regions were observed in the field of view after 1 min, and the fluorescence image (F-image) stabilized within 5 min (Fig. 6c). By adjusting the G-value input color scale of the D-image, it can be clearly observed that after 10 s of reaction, there are various green spots distributed in the field of view. As the reaction proceeded, these nitrite particles gradually diffused and reacted with the coumarin probe, causing the green spots to gradually become fragmented. By mapping the G-value of the D-image of the 10 s reaction, a converted 3D color map showing detailed morphological information was obtained. Through pixel scanning in the selected area, various intensity peaks corresponding to the position of the fluorescent spot can be obtained (Fig. 6d), which verifies the presence of nitrite solid particles. Furthermore, by analyzing the color value of the detected image and the selected green area, it can be observed that both the increased G value and green area were stable after 3 min, accompanied by a negative exponential distribution (Fig. 6e). Thus, it was confirmed that the present hydrogel sensor is capable of detecting trace nitrite particulates in an open environment.

4. Conclusion

In summary, this study proposes a modulating strategy for altering the amine and coupling sites to achieve a colorimetric-fluorescent dual-mode response toward trace nitrite. By analyzing the electrostatic potential of the coumarin probe with different amino substitutions and the corresponding coupling reaction activity at different sites, it is clear that when the amino group is at position 7, the coupling reaction can occur at the ortho- site with the highest binding energy. Correspondingly, its colorimetric-fluorescent dual-mode response in the presence of nitrite was verified to be the large electron-hole separation caused by intermolecular charge transfer interdiction in the twisted molecule conformation. Thus, the probe was proven to have an ultrasensitive dual-mode response towards nitrite with LODs of 98 nM (fluorescent mode) and 629 nM (colorimetric mode) and great specificity to discriminate nitrite from other 15 common anions and interfering substances. Moreover, by loading the probe into the PVA hydrogel to fabricate a sensor, on-site analyses toward nitrite spiked in real samples and qualitative analyses

for trace nitrite particulates were performed. Overall, this site-modulating strategy provides a promising alternative for the ultrasensitive determination of nitrite, and exhibits an important enlightening significance for real-time and on-site analysis toward trace substances from the aspect of molecular conformation regulation.

CRediT authorship contribution statement

Tianshi Zhang: Methodology, Formal analysis, Investigation, Writing - Original Draft, Visualization. **Yuan Liu**: Data Curation, Writing - Review & Editing, Funding acquisition. **Jiguang Li**: Formal analysis, Visualization. **Wenfei Ren**: Validation, Investigation. **Xincun Dou**: Conceptualization, Writing - Review & Editing, Supervision, Project administration, Funding acquisition.

Declaration of Competing Interest

The authors declare that they have no known competing financial interests or personal relationships that could have appeared to influence the work reported in this paper.

Data availability

Data will be made available on request.

Acknowledgments

This work was supported by the Xinjiang International Science & Technology Cooperation Program (2021E01008), the National Natural Science Foundation of China (52172168), the Key Research Program of Frontier Sciences (CAS grant no. ZDBSLY-JSC029), and the Natural Science Foundation of Xinjiang (2022D01E03).

Appendix A. Supporting information

Supplementary data associated with this article can be found in the online version at doi:10.1016/j.snb.2022.133261.

References

[1] S.S. Mirvish, Gastric cancer and salivary nitrate and nitrite, Nature 315 (1985) 461–462.
[2] A.R. Boğa, M. Öztürk, İ.B. Topçu, Using ANN and ANFIS to predict the mechanical and chloride permeability properties of concrete containing GGBFS and CNI, Compos. Part B 45 (2013) 688–696.
[3] H. Su, Y. Cheng, R. Oswald, T. Behrendt, I. Trebs, F.X. Meixner, M.O. Andreae, P. Cheng, Y. Zhang, U. Pöschl, Soil nitrite as a source of atmospheric HONO and OH radicals, Science 333 (2011) 1616–1618.
[4] M.Y.Z. Abouleish, Concentration of selected anions in bottled water in the united arab emirates, Water 4 (2012) 496–509.
[5] X. Zhang, Y.-m Lin, X.-q Shan, Z.-l Chen, Degradation of 2,4,6-trinitrotoluene (TNT) from explosive wastewater using nanoscale zero-valent iron, Chem. Eng. J. 158 (2010) 566–570.
[6] E.J. Johnston, E.L. Rylott, E. Beynon, A. Lorenz, V. Chechik, N.C. Bruce, Monodehydroascorbate reductase mediates TNT toxicity in plants, Science 349 (2015) 1072–1075.
[7] T. Zhang, X. Hu, B. Zu, X. Dou, A march to shape optical artificial olfactory system toward ultrasensitive detection of improvised explosives, Adv. Photonics Res. 3 (2022), 2200006.
[8] Y. Han, R. Zhang, C. Dong, F. Cheng, Y. Guo, Sensitive electrochemical sensor for nitrite ions based on rose-like AuNPs/MoS_2/graphene composite, Biosens. Bioelectron. 142 (2019), 111529.
[9] R. Yang, Y. Lin, J. Yang, L. He, Y. Tian, X. Hou, C. Zheng, Headspace solid-phase microextraction following chemical vapor generation for ultrasensitive, matrix effect-free detection of nitrite by microplasma optical emission spectrometry, Anal. Chem. 93 (2021) 6972–6979.
[10] Y. Hao, Z. Yang, W. Dong, Y. Liu, S. Song, Q. Hu, S. Shuang, C. Dong, X. Gong, Intelligently design primary aromatic amines derived carbon dots for optical dual-mode and smartphone imaging detection of nitrite based on specific diazo coupling, J. Hazard. Mater. 430 (2022), 128393.
[11] J. Zhang, J. Yang, J. Chen, Y. Zhu, K. Hu, Q. Ma, Y. Zuo, A novel propylene glycol alginate gel based colorimetric tube for rapid detection of nitrite in pickled vegetables, Food Chem. 373 (2022), 131678.
[12] X. Wang, E. Adams, A. Van, Schepdael, A fast and sensitive method for the determination of nitrite in human plasma by capillary electrophoresis with fluorescence detection, Talanta 97 (2012) 142–144.
[13] Z. Lin, W. Xue, H. Chen, J.-M. Lin, Peroxynitrous-acid-induced chemiluminescence of fluorescent carbon dots for nitrite sensing, Anal. Chem. 83 (2011) 8245–8251.
[14] S.-S. Li, Y.-Y. Hu, A.-J. Wang, X. Weng, J.-R. Chen, J.-J. Feng, Simple synthesis of worm-like Au–Pd nanostructures supported on reduced graphene oxide for highly sensitive detection of nitrite, Sens. Actuators B Chem. 208 (2015) 468–474.
[15] L. Chiesa, F. Arioli, R. Pavlovic, R. Villa, S. Panseri, Detection of nitrate and nitrite in different seafood, Food Chem. 288 (2019) 361–367.
[16] T.L. Mako, A.M. Levenson, M. Levine, Ultrasensitive detection of nitrite through implementation of n-(1-naphthyl)ethylenediamine-grafted cellulose into a paper-based device, ACS Sens. 5 (2020) 1207–1215.
[17] E. Trofimchuk, Y. Hu, A. Nilghaz, M.Z. Hua, S. Sun, X. Lu, Development of paper-based microfluidic device for the determination of nitrite in meat, Food Chem. 316 (2020), 126396.
[18] P. Singhaphan, F. Unob, Thread-based platform for nitrite detection based on a modified Griess assay, Sens. Actuators B Chem. 327 (2021), 128938.
[19] T. Taweekarn, W. Wongniramaikul, C. Boonkanon, K. Phatthanawiwat, P. Pasitsuparoad, R.J. Ritchie, A. Choodum, Griess-doped polyvinyl alcohol thin film for on-site simultaneous sample preparation and nitrite determination of processed meat products, Food Chem. 389 (2022), 133085.
[20] T. Zhang, X. Hu, B. Zu, X. Dou, Bilayer hydrogel sensor boosted ng-level solid nitrite detection through asymmetrical diffusion construction facilitated colorimetric signal enhancement, Sens. Actuators B Chem. 369 (2022), 132324.
[21] Y. Ke, Y. Liu, B. Zu, D. Lei, G. Wang, J. Li, W. Ren, X. Dou, Electronic tuning in reaction-based fluorescent sensing for instantaneous and ultrasensitive visualization of ethylenediamine, Angew. Chem. Int. Ed. 61 (2022), e202203358.
[22] H. Rau, Spectroscopic properties of organic azo compounds, Angew. Chem. Int. Ed. 12 (1973) 224–235.
[23] G. Bartwal, K. Aggarwal, J.M. Khurana, An ampyrone based azo dye as pH-responsive and chemo-reversible colorimetric fluorescent probe for Al^{3+} in semi-aqueous medium: implication towards logic gate analysis, N. J. Chem. 42 (2018) 2224–2231.
[24] S. Munan, M. Ali, R. Yadav, K. Mapa, A. Samanta, PET- and ICT-based ratiometric probe: an unusual phenomenon of morpholine-conjugated fluorophore for mitochondrial ph mapping during mitophagy, Anal. Chem. 94 (2022) 11633–11642.
[25] K. Liu, M. Qin, Q. Shi, G. Wang, J. Zhang, N. Ding, H. Xi, T. Liu, J. Kong, Y. Fang, Fast and selective detection of trace chemical warfare agents enabled by an esipt-based fluorescent film sensor, Anal. Chem. 94 (2022) 11151–11158.
[26] G. Wang, Z. Wan, Z. Cai, J. Li, Y. Li, X. Hu, D. Lei, X. Dou, Complete inhibition of the rotation in a barrierless tict probe for fluorescence-on qualitative analysis, Anal. Chem. 94 (2022) 11679–11687.
[27] M. Zhao, J. Wang, Z. Lei, L. Lu, S. Wang, H. Zhang, B. Li, F. Zhang, NIR-II pH sensor with a FRET adjustable transition point for in situ dynamic tumor microenvironment visualization, Angew. Chem. Int. Ed. 60 (2021) 5091–5095.
[28] F. Xiao, Y. Li, J. Li, D. Lei, G. Wang, T. Zhang, X. Hu, X. Dou, A family of oligo(p-phenylenevinylene) derivative aggregation-induced emission probes: ultrasensitive, rapid, and anti-interfering fluorescent sensing of perchlorate via precise alkyl chain length modulation, Aggreg. (2022), https://doi.org/10.1002/agt2.260.
[29] Z. Su, Y. Li, J. Li, K. Li, X. Dou, Ultrasensitive dual-mode visualization of perchlorate in water, soil and air boosted by close and stable Pt–Pt packing endowed low-energy absorption and emission, J. Mater. Chem. A 10 (2022) 8195–8207.
[30] Z. Ma, J. Li, X. Hu, Z. Cai, X. Dou, Ultrasensitive, specific, and rapid fluorescence turn-on nitrite sensor enabled by precisely modulated fluorophore binding, Adv. Sci. 7 (2020), 2002991.
[31] H. Bock, G. Rudolph, E. Baltin, J. Kroner, Color and constitution of azo compounds, Angew. Chem. Int. Ed. 4 (1965) 457–471.
[32] H.Y. Lee, X. Song, H. Park, M.-H. Baik, D. Lee, Torsionally responsive c3-symmetric azo dyes: azo−hydrazone tautomerism, conformational switching, and application for chemical sensing, J. Am. Chem. Soc. 132 (2010) 12133–12144.
[33] C. Adamo, V. Barone, Toward reliable density functional methods without adjustable parameters: the PBE0 model, J. Chem. Phys. 110 (1999) 6158–6170.
[34] S. Grimme, S. Ehrlich, L. Goerigk, Effect of the damping function in dispersion corrected density functional theory, J. Comput. Chem. 32 (2011) 1456–1465.
[35] W.J. Hehre, R. Ditchfield, J.A. Pople, Self-consistent molecular-orbital methods.12. Further extensions of Gaussian-type basis sets for use in molecular-orbital studies of organic-molecules, , J. Chem. Phys. 56 (1972) 2257–2261.
[36] S. Miertus, E. Scrocco, J. Tomasi, Electrostatic interaction of a solute with a continuum – a direct utilization of abinitio molecular potentials for the prevision of solvent effects, Chem. Phys. 55 (1981) 117–129.
[37] M.J. Frisch, G.W. Trucks, H.B. Schlegel, G.E. Scuseria, M.A. Robb, J.R. Cheeseman, et al., Gaussian 09, Revision A.02, Wallingford, CT, 2016.
[38] Z. Liu, T. Lu, Q. Chen, An sp-hybridized all-carboatomic ring, cyclo[18]carbon: electronic structure, electronic spectrum, and optical nonlinearity, Carbon 165 (2020) 461–467.
[39] J.S. Murray, P. Politzer, Electrostatic Potentials: Chemical Applications, Encyclopedia of Computational Chemistry, 2022.
[40] P. Sjoberg, J.S. Murray, T. Brinck, P. Politzer, Average local ionization energies on the molecular surfaces of aromatic systems as guides to chemical reactivity, Can. J. Chem. 68 (1990) 1440–1443.
[41] T. Lu, F.W. Chen, Multiwfn: a multifunctional wavefunction analyzer, J. Comput. Chem. 33 (2012) 580–592.

[42] W. Humphrey, A. Dalke, K. Schulten, VMD: visual molecular dynamics, J. Mol. Graph. Model. 14 (1996) 33–38.
[43] J. Li, Z. Ma, D. Lei, B. Zu, X. Dou, Precisely modulated electrostatic attraction to the recognition site for on-site ultrafast visualization of trace hydrazine, Cell Rep. Phys. Sci. 3 (2022), 100878.
[44] W.H. Organization, Guidelines for drinking-water quality: second addendum. Vol. 1, Recommendations: World Health Organization; 2008.
[45] R. Tawa, S. Hirose, Application of simplified complementary tristimulus colorimetry to chemical kinetics in solution – II Determination of rate constants of consecutive irreversible first-order reactions, Talanta 27 (1980) 759–761.
[46] P.M. Nowak, P. Kościelniak, What color is your method? Adaptation of the RGB additive color model to analytical method evaluation, Anal. Chem. 91 (2019) 10343–10352.

Xincun Dou obtained his Ph.D. in Material Physics and Chemistry from the Institute of Solid State Physics of the Chinese Academy of Sciences (CAS) in 2009. Following post-doctoral work at Nanyang Technological University in Singapore, he joined Xinjiang Technical Institute of Physics & Chemistry, CAS in 2011. His research interests focus on the exploratory design of optoelectronic nanomaterials and devices, micro nanosensors, colorimetric sensing and analysis, trace explosives detection and analysis technology.

Yuan Liu received her Ph.D. in major of Molecular Sciences from Macquarie University, Australia in February 2021. She joined Xinjiang Technical Institute of Physics & Chemistry, CAS in 2021. Her current research focus is trace substance analysis based on optical sensing technology, nanomaterial construction and its application in sensor development.

Tianshi Zhang received his B.S. in School of the Gifted Young from University of Science and Technology of China in 2017. He is currently working toward the Ph.D. degree in Prof. Dou's group from Xinjiang Technical Institute of Physics & Chemistry, CAS. His current research interests include optical chemosensors towards improvised explosives and functionalized hydrogels.

Jiguang Li received his B.Eng. in School of Material Science and Engineering from University of Jinan in 2018. He is currently working toward the Ph.D. degree in Prof. Dou's group from Xinjiang Technical Institute of Physics & Chemistry, CAS. His current research interests focus on theoretical and computational chemistry for optical probes.

Wenfei Ren received her B.Eng. in Safety Engineering from North University of China in 2018. She is currently working toward the Ph.D. degree in Prof. Dou's group from Xinjiang Technical Institute of Physics & Chemistry, CAS. Her research interests focus on the detection of improvised explosives.